Adaptive Transmission Design for Rechargeable Wireless Sensor Network With a Mobile Sink

Xiaolong Lan, *Member, IEEE*, Yongmin Zhang, *Member, IEEE*, Lin Cai, *Fellow, IEEE*, and Qingchun Chen, *Senior Member, IEEE*

***Abstract*—In this article, we aim at maximizing the data gathering performance of the rechargeable wireless sensor network, where a mobile sink moves along the predefined path to charge sensor nodes through a wireless energy transfer technique and gather data from them. First, we show how to transform the original time-average optimization problem into a queue stability one by using the Lyapunov optimization framework, then we show how to decompose it into multiple subproblems by using the optimization decomposition. A distributed speed control and routing algorithm was proposed to reduce the computing load of the mobile sink and to obtain the near-optimal solution for data collection. Our analysis shows that there is an inherent tradeoff between the network utility and the average data queuing size, and the proposed adaptive transmission scheme can achieve the near-optimal network utility when a certain queueing delay can be tolerated.**

***Index Terms*—Distributed algorithm, mobile sink, network utility, rechargeable wireless sensor networks, wireless energy transfer.**

I. Introduction

WIRELESS sensor networks (WSNs) are mostly powered by batteries, which can only operate for a limited time since the limited battery capacity. Wireless energy transfer techniques have been shown to provide an alternative approach to prolong the lifetime of WSNs [1]–[10]. Unlike energy harvesting techniques based on natural sources, wireless energy transfer techniques can provide reliable and permanent energy resources for energy-constrained devices without being affected by environmental changes. Wireless energy transfer includes three methods: 1) magnetic resonance coupling; 2) inductive coupling; and 3) radio-frequency (RF) energy transfer [10]. The first two wireless energy transfer techniques are near-field energy transfer with high conversion efficiency, but they need to calibrate and align coils/resonators between transmitters and receivers, not suitable for remote and mobile charging. The RF energy transfer is considered as a far-field energy transfer technique. Thus, compared with the first two techniques, the RF energy transfer is more suitable for supplying power to a larger number of devices deployed in a wide area, such as WSNs and the Internet of Things. However, RF energy transfer techniques suffer from a low energy efficiency caused by the large-scale fading of RF signals. Thus, how to adequately charge the WSNs through the RF energy transfer technique and how to improve the energy transfer efficiency will impose technical challenges.

To tackle the inefficiency of RF energy transfer, the energy beamforming technique in [18]–[23] can be used. Moreover, in such RWSNs, rechargeable sensors are deployed along both sides of the predefined road for environmental monitoring, and a mobile sink moves along the road to gather sensing data from sensors periodically, and each sensor is powered by RF energy transferred from the mobile sink only. There is an interesting "doubly near–far" phenomenon in this RWSNs, that is, a sensor far away from the road harvests less energy while it has to transmit sensing data with more energy to overcome the larger path loss. To address this issue, some sensors close to the road can use part of its harvested energy to help other sensors forward sensing data such that the overall network performance will be improved. Thus, how to design efficient energy beamforming and routing scheme is our primary research motivation in this article.

On the other hand, the required transmission energy consumption increases as the transmission distance increases. The harvested energy and the total amount of transmitted data will be affected by the speed of the mobile sink. There is an intuitive method to improve the entire network performance by letting the mobile sink decelerate (accelerate) in dense (sparse) area of sensors. Thus, how to effectively control the speed of the mobile sink to further improve the network performance is our second research motivation.

In this article, focusing on RWSNs with a mobile sink, we consider a realistic scenario, where each sensor is equipped with a data buffer and energy storage to buffer sensing data

Manuscript received December 2, 2019; revised March 24, 2020 and May 24, 2020; accepted June 1, 2020. Date of publication June 9, 2020; date of current version September 15, 2020. The work of Xiaolong Lan was supported in part by the National Natural Science Foundation of China (NSFC) under Grant 61771406, and in part by the Chinese Scholarship Council. The work of Yongmin Zhang was supported by NSFC under Grant 61702450. The work of Lin Cai was supported in part by NSFC under Grant 61828301, in part by the Natural Sciences and Engineering Research Council of Canada, and in part by Compute Canada. The work of Qngchun Chen was supported in part by NSFC under Grant 61771406, in part by the Lingnan Yingjie Project by Guangzhou Municipal Government, and in part by International Science and Technology Thematic Collaboration Program by Department of Science and Technology, Guangdong Province. *(Corresponding author: Qingchun Chen.)*

Xiaolong Lan is with the College of Cybersecurity, Sichuan University, Chengdu 610065, China (e-mail: xiaolonglan1112@gmail.com).

Yongmin Zhang is with the Department of Computer Science, Central South University, Changsha 410083, China (e-mail: zhangyongmin@csu.edu.cn).

Lin Cai is with the Department of Electrical and Computer Engineering, University of Victoria, Victoria, BC V8W 3P6, Canada (e-mail: cai@ece.uvic.edu).

Qingchun Chen is with the Research Center of Intelligent Communication Engineering, Guangzhou University, Guangzhou 510006, China (e-mail: qcchen@gzhu.edu.cn).

Digital Object Identifier 10.1109/JIOT.2020.3001034

and store the harvested energy temporarily. To maximize the network utility, the adaptive transmission design problem is formulated to consider the data and energy queue causality, the peak transmit power constraint, the average speed constraint of the mobile sink, as well as the link capacity constraint. The contributions of this article can be briefly summarized as follows.

1) We propose an adaptive transmission scheme (ATS) to substantially improve the network utility by carefully devising energy beamforming, rate control, speed control of the mobile sink, and routing strategy. Moreover, it is unveiled that the energy transfer efficiency can be effectively improved by designing the appropriate energy beamforming scheme and controlling the speed of the mobile sink.
2) We obtain the optimal energy beamforming and rate control strategy. By transforming the linear programming problem of the speed control and routing design into the quadratic programming problem via a proximal minimization algorithm, asymptotic optimal speed control and routing are obtained as well. To reduce the computation payload of the mobile sink, a distributed speed control and routing algorithm is developed to obtain the near-optimal solution for data collection.
3) Our analysis shows that there is an inherent tradeoff between the average data queuing size and the network utility, and the proposed ATS can achieve the near-optimal network utility when a certain queueing delay can be tolerated.

The remainder of this article is organized as follows. In Section II, a literature survey is presented to introduce the motivations and the related works. The system model and problem statement of the considered RWSNs are presented in Section III. The utility maximization problem and ATS design are presented in Section IV. Numerical analysis and simulation results are presented in Section V to verify the effectiveness of this article, followed by concluding remarks and further research issues in Section VI.

Notations: All boldface letters represent vectors (lowercase) or matrices (uppercase). The superscripts $(\cdot)^{\mathrm{T}}$ and $(\cdot)^{\mathrm{H}}$ indicate the transposition and the conjugate transposition, respectively. $|z|$ represents the magnitude of a complex variable z, $\|\mathbf{z}\|$ denotes the Euclidean norm of a complex vector $\mathbf{z}$, and $\mathrm{tr}(\mathbf{A})$ represents the trace of a matrix $\mathbf{A}$, where $\mathbf{A} \succeq 0$ means that matrix $\mathbf{A}$ is positive semidefinite. $\mathbf{A} = \mathrm{diag}(\mathbf{v})$ denotes a square diagonal matrix with the elements of vector $\mathbf{v}$ on the main diagonal.

II. Related Works

Energy harvesting techniques that leverage renewable energy and wireless energy transfer have recently attracted considerable attention as they can prolong the lifetime of WSNs. Zhang *et al.* [17] proposed a distributed sensing rate and routing control algorithm to maximize the data gathering rate in RWSNs while guaranteeing the fairness of the network. Energy-aware routing with distributed energy replenishment was considered in [27], which aimed at designing the routing algorithms to optimally utilize the available energy in the presence of energy constraints. In addition, the problems of network utility maximization for data gathering in RWSNs have been considered in [4], [5], and [13]–[16]. Meanwhile, a mobile sink can alleviate traffic flow bottleneck in the WSNs, and potentially increase the lifetime of the WSNs since its changing locations result in the lower energy consumption when the sink is close to the sensors [24]–[26], [28]. Existing works on utilizing mobile sink to improve the lifetime of the RWSNs can be briefly categorized as follows.

A. Energy Harvesting Leveraging Renewable Energy

The problem of data gathering in RWSNs with a constant speed mobile sink was studied in [15], which aimed at maximizing the data gathering rate of the mobile sink while guaranteeing the network fairness. In [13], in order to circumvent communication bottlenecks caused by spatial energy variations, a mobile sink was employed to gather data from sensors and to balance energy consumption in WSNs. The data collection throughput maximization problem was studied in [12] for WSNs with a mobile sink. In [11], a general framework was proposed to maximize the network throughput in energy harvesting WSNs by determining the optimal distance or sink speed, and it is shown that the network throughput can be improved noticeably by optimizing the speed of the mobile sink. However, since the harvested energy leveraging renewable energy sources depends only on the surrounding environment and is particularly sensitive to changes in the environment, the total amount of energy collected may become unstable and is independent of the speed of the mobile sink. Hence, these speed control algorithms based on natural energy sources are not suitable for the RWSNs with wireless energy transfer.

B. Wireless Energy Transfer Based on Magnetic Resonance Coupling

Shi *et al.* [1] and Xie *et al.* [2] studied the scenario in which a mobile charging vehicle periodically travels inside the WSNs, and the static data gathering is assumed at every sensor node and each sensor battery is assumed to be recharged wirelessly. The proposed scheme aimed at maximizing the ratio of wireless charging vehicle vacation time over cycle time. The scenario with one data gathering vehicle and multiple mobile charging vehicles traversing the network was studied in [29] to balance energy consumption and to reduce data latency. The problem of the anchor point selection was studied in [4] and [5], where the mobile sink periodically chooses the locations for a subset of sensors as their anchor points, thus the mobile sink sequentially visits and charges the sensors at these locations and collects data from nearby sensors. Although magnetic resonance coupling-based wireless energy transfer techniques can efficiently transfer energy, it requires calibration and alignment of coils. Thus, it is not suitable for the considered dense WSNs. In addition, most existing works about the resonant-based wireless charging mainly focus on the path planning problem of the mobile sink, without considering how to efficiently control the speed of the mobile sink to further improve the network performance.

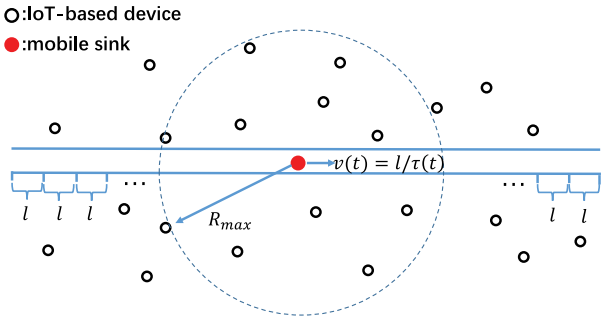

Fig. 1. RWSN with wireless energy transfer and a mobile sink.

C. Wireless Energy Transfer Based on the RF Signal

Han *et al.* [9] studied a joint energy replenishment and data collection problem in WRSNs, where two mobile chargers were employed to improve energy efficiency. The problem of the mobile sink powers the sensor by RF signal and then gathers sensory data from the sensor was investigated in [30], in which the harvest-and-use scheme and the harvest-and-store scheme were proposed according to whether there is energy storage at the sensor. It is disclosed that with the help of energy storage, the network performance can be significantly improved through opportunistic energy transfer. A joint routing and mobile charging scheme was proposed in [31] to improve the network energy utilization and prolong the lifetime of the network. However, these works only focus on exploiting mobility of the sink to extend the network lifetime and do not take the energy beamforming design into consideration of the transmission design for the WSNs. How to further improve the network performance by jointly controlling the speed of the mobile sink and designing energy beamforming is still an open problem, which motivates our work in this article.

III. System Model and Problem Statement

As shown in Fig. 1, we consider an RWSN, in which one mobile sink s travels along a predefined path at a constant speed within several equal length distances and K rechargeable sensors are randomly deployed along both sides of the path. Each sensor node is powered by RF wireless energy transferred from the mobile sink only. It is assumed that the mobile sink is provisioned with $N+1$ antennas, in which N transmit antennas are used for wireless energy transfer and one receive antenna is used to receive data from the sensors. We assume that each sensor is equipped with two antennas, one of which is used for transmitting sensory data and the other one is used for harvesting energy. In addition, we assume that each sensor is equipped with a data buffer and energy storage to store sensing data and the harvested energy, respectively. For the considered RWSN, two transmission modes are assumed: 1) the RF energy transmission mode, in which the mobile sink transmits RF energy beam to the sensors for harvesting energy and 2) the data transmission mode, in which each sensor transmits its collected data to the mobile sink. It is further assumed that the energy transmission mode and the data transmission mode can be performed in different frequency bands such that there is no interference between the data signal and the energy beam, namely, they can be operated at the same time.

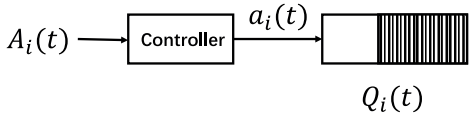

Fig. 2. Control model.

It is assumed that the mobile sink s moves along the predefined path periodically to gather sensory data from sensors directly or in a multihop manner. The path length L can be subdivided into several equal length distances l. Let us denote the time duration for s to travel distance l as a time slot. Since s can change its speed at different time slots, the duration changes accordingly. Denote $\tau(t)$ and $v(t)$ the time duration and the speed of s in the tth time slot, respectively. Therefore, we have $\tau(t) = [l/v(t)]$ and the total number of slots in each period is $N_T = (L/l)$. We assume that l is small enough such that the channel fading variation and the distances between the sink and all sensors can be approximately assumed to be constant within each time slot.[1] Scheduling and data transmissions are subslot based with a constant duration, which is independent of $\tau(t)$. In the practical system, a subslot is much shorter than $\tau(t)$. However, all the subslots within one-time slot share the same scheduling decision given the constant transmission distance. In addition, to meet the delay-sensitive traffic requirements, it is further assumed that the duration of each period will be no larger than T_{tol}, which indicates that the average speed of s is no less than (L/T_{tol}).

We consider a controller shown in Fig. 2, which can control the amount of sensing data placed in the data buffer in each time slot. Let $A_i(t)$ denote the total amount of data sensed by sensor i at time slot t. Let $a_i(t)$ denote the amount of sensing data for sensor i that are actually placed in the corresponding data buffer at slot t. Let $E_i(t)$ and $Q_i(t)$ denote the energy and data queue state for sensor i at time slot t, respectively. The energy storage size of sensor i is expressed by $\hat{E}_i$. In this article, it is assumed that the data buffer size is large enough such that the overflow probability can be negligible. In Theorem 1 and Section V, we will prove and verify that there is an upper bound on the size of the data buffer, i.e., no overflow happens as long as the data buffer is large enough. For simplicity, it is assumed that the mobile sink is equipped with a large enough data buffer to store the data received from the sensors and has sufficient energy to charge all the sensors. For the sake of clarity, the symbols used throughout this article are summarized in Table I.

[1]It is shown in [10] that in RF energy harvesting, radio signals with a frequency range from 300 GHz to as low as 3 KHz are used as a medium to carry energy in the form of electromagnetic radiation. In this article, we assume a comparatively low carrier frequency for the RF energy harvesting such that the channel fading and phase variations associated with the target sensor within a distance change of l can be negligible. In practical applications, we should take into consideration of the tradeoff among the utilized radio signal frequency for energy harvesting, the mobile sink size, the required beamforming vector update frequency, and the realized energy beamforming performance.

TABLE I
SYMBOL NOTATION LIST

Symbol	Definition
K	The number of rechargeable sensors
N	The number of antennas used for RF energy transfer
$(x_s(t), 0)$	Location of mobile sink s at slot t
(x_i, y_i)	Location of sensor i
L	The pre-defined path length
l	Distance traveled by sink s in each time slot
$v(t)$	Speed of sink s at slot t
$\overline{v}$	Maximum speed allowed by sink s
$\underline{v}$	Minimum speed allowed by sink s
$\tau(t)$	The duration of the t-th slot
N_T	The total number of time slots in each round
T_{tol}	Maximum average duration of each period can be tolerated
$d_{ij}(t)$	Distance between node i and node j at slot t
$R_{\max}$	Maximum charging distance
$\mathcal{K}$	Set of sensors that can be charged by sink s
$\mathbf{g_{is}}(t)$	The channel coefficient vector between mobile sink s and sensor i
η	The energy conversion efficiency
$A_i(t)$	The total amount of data sensed by sensor i at slot t
$a_i(t)$	The amount of data for sensor i that are actually placed in the corresponding data buffer at slot t
$f_{ij}(t)$	The total amount of sensing data transmitted from node i to node j through the link (i, j) at slot t
E_i^{rx}	Energy consumption of receiving one bit for sensor i
$E_{ij}^{tx}(t)$	Energy consumption of transmitting one bit through the link (i, j) at slot t
$\hat{E}_i$	Energy storage size of sensor i
$E_i(t)$	The state of energy queue for sensor i at slot t
$Q_i(t)$	The state of data queue for sensor i at slot t
$Z(t)$	The state of virtual queue for speed control of sink s at slot t
$\mathbf{w(t)}$	Energy beamforming vector at slot t
$H_i(t)$	Harvested energy by sensor i at slot t
$C_i(t)$	Energy consumption of sensor i at slot t
W_{ij}	The transmit bandwidth of link (i, j)
$R_{xi}(t)$	The total amount of data that are placed in the data buffer of sensor i at slot t
$T_{xi}(t)$	The total amount of data transmitted by sensor i at slot t
$\bar{a}_i$	The average amount of the sensing data that can be transmitted successfully by sensor i
$U(\bar{a}_i)$	The network utility function of sensor i

A. Energy Transmission and Consumption Model

Let $(x_i, y_i), i = 1, 2, \ldots, K$, denote the location of sensor i. Let $d_{ij}(t)$ denote the distance between node i and node j at slot t. Without loss of generality, it is assumed that sink s periodically moves along a predefined straight path with $y = 0$. Thus, the location of sink s at time slot t is $(x_s(t), 0)$ and the distance between sensor i and sink s is expressed as

$$d_{is}(t) = \sqrt{(x_s(t) - x_i)^2 + y_i^2} \tag{1}$$

where $x_s(t) = (t - \lfloor (t/N_T) \rfloor N_T) l$. Let $R_{\max}$ denote the maximum charging distance, i.e., sensor i can harvest energy from mobile sink only when $d_{is}(t) \leq R_{\max}$. Therefore, at slot t, the set of the sensors that can be charged by sink s is given by

$$\mathcal{K}(t) = \left\{ k \;\middle|\; d_{is}(t) \leq R_{\max} \quad \forall i \in \{1, 2, \ldots, K\} \right\}. \tag{2}$$

To guarantee all the sensors can harvest energy from sink s, we assume that the vertical distances between the straight path and all sensors are less than $R_{\max}$, i.e., $y_i \leq R_{\max}$ $\forall i$. Since mobile sink s is equipped with N antennas deployed in a uniform linear array, the sensor can be powered by RF energy beams such that the energy efficiency can be improved. It is assumed that sink s can change the beamforming vector in each slot. At time slot t, we have the following energy beamforming vector:

$$\mathbf{w}(t) = (w_1(t), w_2(t), \ldots, w_N(t))^{\mathrm{T}} \in \mathbb{C}^{N \times 1}. \tag{3}$$

Therefore, the transmit power of sink s at time slot t is $P_s(t) = \|\mathbf{w(t)}\|^2$ and the channel coefficient vector between mobile sink s and sensor i is given by [3]

$$\mathbf{g_{is}}(t) = \sqrt{\frac{G_s G_r}{L_p}} \frac{\lambda}{4\pi (d_{is}(t) + \beta)} \left[1 \;\; e^{\mathrm{j}\theta_{i,t}} \;\; \cdots \;\; e^{\mathrm{j}(N-1)\theta_{i,t}} \right] \tag{4}$$

where G_s and G_r are the antenna gain of mobile sink s and sensors, respectively. L_p is the polarization loss, λ is the signal wavelength, and β is a parameter to adjust Friis' free space equation for short distance transmission. $\theta_{i,t} = -([2\pi d^{an} \sin(\psi_{i,t})]/\lambda)$, d^{an} is the spacing between successive antenna elements at sink s and $\psi_{i,t} = \arcsin(y_i/[d_{is}(t)])$ is the direction of sensor i to sink s.[2] Therefore, the received signal at sensor i can be expressed as

$$y_i(t) = \mathbf{g_{is}}(t)\mathbf{w}(t) + n_i \quad \forall i \in \mathcal{K}(t) \tag{5}$$

where n_i is the Gaussian noise. We assume that the harvested energy from the noise at sensors is negligible and thus ignored. Thus, the harvested energy of sensor i in time slot t is expressed as

$$H_i(t) = \begin{cases} \eta \tau(t) |\mathbf{g_{is}}(t)\mathbf{w}(t)|^2, & \text{if } i \in \mathcal{K}(t) \\ 0, & \text{otherwise} \end{cases} \tag{6}$$

where η denotes the energy conversion efficiency. We assume the same energy consumption model for transmitting data and receiving data in [32]. When sensor i needs to transmit 1-b sensing data to its next-hop j at time slot t, the energy consumption for data transmission is given by

$$E_{ij}^{tx}(t) = E_{\text{elec}} + E_{\text{amp}} d_{ij}^2(t) \tag{7}$$

[2]It should be addressed that when the channel coefficient vector $\mathbf{g_{is}}(t)$ is no longer known, signaling between the mobile sink and sensors is needed to acquire $\mathbf{g_{is}}(t)$, which requires proper channel estimate design and incurs a communication overhead similar to other beamforming communication systems.

where E_{elec} and E_{amp} are nonnegative constants. The energy consumption used to receive 1 b of data for sensor i is $E_i^{rx} = E_{\text{elec}}$. Given the movement of sink s, the energy consumption of directly transmitting from sensor i to mobile sink s will change with slot t. However, the distance $d_{ij} (j \neq s)$ between sensor i and sensor j is fixed, which leads to constant energy consumption for transmitting 1 b between sensors. Similar to [4], [7], and [9], in this article, we only take into account the energy consumption used to transmit and receive data because they dominate energy consumption.

B. Data Transmission Model

Since some sensors are far away from the road, this leads to less energy harvested by these sensors, and they have to consume more energy to transmit data to sink s directly. Therefore, some sensors close to the road can use part of their harvested energy to help other sensors forward sensing data to sink s. In this way, the overall network performance may be improved. For simplicity, it is assumed that some underlying protocols can be used to eliminate the signal interference among nodes, for instance, FDMA.

To improve energy efficiency, sensor j can serve as the next hop of sensor i to forward its sensing data, if and only if the following conditions are met [15].

1) $d_{ij} < |y_i|$, which indicates the distance between sensor i and sensor j is no greater than the distance between sensor i and the road.
2) $|y_i| > |y_j|$, which guarantees that sensor j as the next hop must be closer to the road than sensor i.

Only when the above two conditions are met, sensor i can consume less energy to transmit sensing data. Let $O(i)$ denote a set of the sensors that can act as the relay to help sensor i forward sensor data. If $d_{ij} < |y_i|$ and $|y_i| > |y_j|$, $j \in O(i)$; otherwise, $j \notin O(i)$.

Let $f_{ij}(t)$ denote the amount of sensing data transmitted from node i to node j through the link (i, j) at time slot t. The amount of data transmitted is limited by the corresponding link capacity. Let W_{ij} denote the transmit bandwidth of the link (i, j). Therefore, $f_{ij}(t)$ satisfies the following constraint [5], [15]:

$$0 \leq f_{ij}(t) \leq W_{ij}\tau(t). \tag{8}$$

In slot t, sensor i can act as a relay to receive the sensing data from other sensors, and the total amount of data placed in the data buffer at sensor i can be expressed as

$$R_{xi}(t) = \sum_{j:i\in O(j)} f_{ji}(t) + a_i(t). \tag{9}$$

The total amount of sensory data transmitted by sensor i in time slot t is given by

$$T_{xi}(t) = \sum_{j:j\in O(i)\cup\{s\}} f_{ij}(t). \tag{10}$$

Therefore, the total energy consumption of sensor i in the tth time slot can be expressed as

$$C_i(t) = \sum_{j:i\in O(j)} f_{ji}(t)E_i^{rx} + \sum_{j:j\in O(i)\cup\{s\}} f_{ij}(t)E_{ij}^{tx}(t). \tag{11}$$

The energy storage and data buffer at sensor i can be updated as follows:

$$E_i(t+1) = \min\left[(E_i(t) + H_i(t) - C_i(t))^+, \hat{E}_i\right] \tag{12}$$

$$Q_i(t+1) = (Q_i(t) + R_{xi}(t) - T_{xi}(t))^+ \tag{13}$$

where $(\cdot)^+ = \max\{\cdot, 0\}$.

IV. Utility Maximization Problem Formulation and Adaptive Transmission Scheme Design

A. Problem Formulation

Let $\bar{a}_i = \lim_{M\to\infty}(1/M)\sum_{t=0}^{M-1} a_i(t), i = 1, 2, \ldots, K$, denote the average amount of the sensing data that can be transmitted successfully by sensor i. $U(\bar{a}_i)$ denotes the network utility function of sensor i, which is a continuous differentiable and monotonically increasing concave function for $\bar{a}_i$. The average amount of the sensing data of RWSN can be maximized if we set $U(\bar{a}_i) = \bar{a}_i$. The fairness of network can be maintained if we set $U(\bar{a}_i) = \log(\bar{a}_i)$.

In this article, our goal is to maximize the network utility subjects to the energy and data queue causality, the peak transmission power constraint, the average speed constraint of mobile sink s, and the link capacity constraint. Moreover, arrival rate control, energy beamforming design, speed control of the mobile sink, and routing design are jointly considered to maximize the network utility. Therefore, the network utility maximization problem can be formulated as follows:

$$\mathbf{P0}: \max_{\mathbf{w}(t),a_i(t),f_{ij}(t),\tau(t)} \sum_{i=1}^{K} U(\bar{a}_i)$$

$$C1: Q_i(t+1) = (Q_i(t) + R_{xi}(t) - T_{xi}(t))^+ \quad \forall\, i, t$$

$$C2: E_i(t+1) = \min\left[(E_i(t) + H_i(t) - C_i(t))^+, \hat{E}_i\right] \quad \forall\, i, t$$

$$C3: \lim_{M\to\infty}\frac{1}{M}\sum_{t=0}^{M-1}\tau(t) \leq \frac{T_{\text{tol}}}{N_T}$$

$$C4: \frac{l}{\bar{v}} \leq \tau(t) \leq \frac{l}{\underline{v}} \quad \forall t$$

$$C5: 0 \leq \|\mathbf{w}(t)\|^2 \leq P_{\max}^s \quad \forall t$$

$$C6: 0 \leq a_i(t) \leq A_i(t) \quad \forall i, t$$

$$C7: 0 \leq f_{ij}(t) \leq W_{ij}\tau(t) \quad \forall i, j, t$$

$$C8: C_i(t) \leq E_i(t) \quad \forall i, t$$

$$C9: T_{xi}(t) \leq Q_i(t) \quad \forall i, t$$

where $\underline{v}$ and $\bar{v}$ denotes the allowed minimum speed and the allowed maximum speed for the mobile sink, respectively. $P_{\max}^s$ is the allowed peak transmit power of sink s. Note that the distance traveled by sink s in each slot is the same, so the speed of sink s can be determined once the duration of each slot is given. Therefore, in our formulated optimization problem **P0**, we convert the speed control of sink s into optimizing the duration of each slot. Constraints C1 and C2 represent the actual data and energy queue causality constraint, respectively. Constraint C3 indicates that the average duration of each slot will not be larger than (T_{tol}/N_T). Constraint C4 indicates the speed limit of the mobile sink. Constraint

C5 stands for the peak transmit power constraint at sink s. Constraint C6 represents that the amount of data actually placed in the data buffer does not exceed that the sensor can sense in each slot. Constraint C7 stands for the corresponding link capacity constraint. Constraint C8 represents that the energy consumption of sensor i cannot exceed the energy that is stored in the energy storage in any slot. Constraint C9 indicates that the sensing data transmitted by sensor i cannot exceed the data stored in the data buffer in any slot.

B. Virtual Queue

To make the average duration of each slot be no larger than (T_{tol}/N_T), i.e., the average speed of sink s cannot be smaller than (L/T_{tol}). We define $Z(t)$ as the virtual queue for the speed control of sink s. The virtual queue evolution is given by

$$Z(t+1) = \left(Z(t) + \tau(t) - \frac{T_{\text{tol}}}{N_T}\right)^+ \quad \forall t. \tag{14}$$

Note that the length of the virtual queue $Z(t)$ increases as $\tau(t)$ increases, which indicates that we should accelerate the speed of sink s to ensure that constraint C3 is satisfied when $Z(t)$ becomes larger.

Lemma 1: If the data queue $Q_i(t), i = 1, 2, \ldots, K$, and the virtual queue $Z(t)$ are both rate stable, i.e., $\lim_{M\to\infty}([Q_i(M)]/M) = \lim_{M\to\infty}[Z(M)/M] = 0$, then

$$\lim_{M\to\infty}\frac{1}{M}\sum_{t=0}^{M-1} R_{xi}(t) \le \lim_{M\to\infty}\frac{1}{M}\sum_{t=0}^{M-1} T_{xi}(t) \quad \forall i \tag{15}$$

$$\lim_{M\to\infty}\frac{1}{M}\sum_{t=0}^{M-1} \tau(t) \le \frac{T_{\text{tol}}}{N_T} \quad \forall i. \tag{16}$$

Proof: See Appendix A. ∎

Lemma 1 indicates that the average speed constraint of sink s can be transformed into a queue stability problem. Moreover, (15) indicates that all the sensing data stored in the data buffer can be sent out if the data queue is stable, i.e., the flow conservation can be guaranteed. Therefore, **P0** can be transformed into maximizing the network utility under the condition that all the queues are stable, which can be effectively solved by employing the Lyapunov optimization framework.

C. Lyapunov Optimization Framework

According to the energy queue state $E_i(t)$, the data queue state $Q_i(t)$, and virtual queue $Z(t)$, we define the quadratic Lyapunov function as follows:

$$L(\Theta(t)) = \frac{1}{2}\sum_{i=1}^{K}\left[\mu_1\left(\hat{E}_i - E_i(t)\right)^2 + \mu_2 Q_i(t)^2\right] + \frac{\mu_3}{2}Z(t)^2 \tag{17}$$

where $\Theta(t) = [E_i(t), Q_i(t), Z(t)]$ denotes the concatenated vector of all queues. μ_1, μ_2, and μ_3 are nonnegative weighting coefficients. The Lyapunov function $\Theta(t)$ measures the size of all queues at slot t, which increases as $Q_i(t)$ and $Z_i(t)$ increase, or with the decrease of $E_i(t)$. The Lyapunov drift represents the change of the Lyapunov function between two consecutive time slots, which is defined as

$$\Delta(\Theta(t)) = \mathbb{E}[L(\Theta(t+1)) - L(\Theta(t))|\Theta(t)] \tag{18}$$

where $\mathbb{E}$ denotes the expectation. First, we should minimize the Lyapunov drift to stabilize all queues. At the same time, our goal is to maximize the network utility. Since the utility function is a continuous differentiable and monotonically increasing concave function, based on Jensen's inequality, we have

$$\lim_{M\to\infty}\frac{1}{M}\sum_{t=0}^{M-1} U(a_i(t)) \le U(\bar{a}_i). \tag{19}$$

This indicates that the utility function evaluated at the time average $\bar{a}_i$ is no less than the time average of $U(a_i(t))$. Our transmission control decision is to maximize $\sum_{i=1}^{K}(1/M)\sum_{t=0}^{M-1}U(a_i(t))$ instead of maximizing $\sum_{i=1}^{K}U(\bar{a}_i)$ directly. It provides the lower bound of the optimal control scheme, which has important guidance significance for the actual transmission control design. Therefore, on the basis of the Lyapunov optimization framework, we can minimize the following Lyapunov drift-plus-penalty in each slot:

$$\Delta(\Theta(t)) - V\sum_{i=1}^{K}\mathbb{E}[U(a_i(t))|\Theta(t)] \tag{20}$$

where V is a nonnegative control parameter. As will be shown later that by adjusting V, we can achieve a reasonable tradeoff between the network utility and the average data queuing size.

Lemma 2: The Lyapunov drift-plus-penalty can be upper bounded by

$$\begin{aligned}
&\Delta(\Theta(t)) - V\sum_{i=1}^{K}\mathbb{E}[U(a_i(t))|\Theta(t)] \\
&\le B + \sum_{i=1}^{K}\Big\{\mu_1\Big(\hat{E}_i - E_i(t)\Big)\mathbb{E}[C_i(t) - H_i(t)|\Theta(t)] \\
&\qquad + \mu_2 Q_i(t)\mathbb{E}\big[R_{xi}(t) - T_{xi}(t)|\Theta(t)\big]\Big\} \\
&\quad + \mu_3 Z(t)\mathbb{E}\left[\tau(t) - \frac{T_{\text{tol}}}{N_T}|\Theta(t)\right] - V\sum_{i=1}^{K}\mathbb{E}[U(a_i(t))|\Theta(t)]
\end{aligned} \tag{21}$$

where $B = (1/2)\{\sum_{i=1}^{K}[\mu_1(\hat{H}_i^2 + \hat{C}_i^2) + \mu_2(\hat{R}_{xi}^2 + \hat{T}_{xi}^2)] + \mu_3(l/\underline{v})^2 + \mu_3(T_{\text{tol}}/N_T)^2\}$. $\hat{H}_i^2$, $\hat{C}_i^2$, $\hat{R}_{xi}$, and $\hat{T}_{xi}$ denote the maximum harvested energy, the maximum energy consumption, the maximum amount of sensing data for sensor i placed in data buffer, and the maximum amount of data transmitted by sensor i, respectively.

Proof: See Appendix B. ∎

Lemma 2 provides us with an upper bound on the Lyapunov drift-plus-penalty, and thus our transmission control decisions are to minimize the Lyapunov drift-plus-penalty upper bound instead of the Lyapunov drift-plus-penalty directly.

D. Adaptive Transmission Scheme Design

1) Problem Transformation: Based on the Lyapunov optimization framework, time-average constraints can be transformed into a queue stability problem by minimizing the upper bound of Lyapunov drift-plus-penalty. Next, we will establish a practical arrival rate control, energy beamforming design, speed control of sink s, and routing design to maximize the network utility while guaranteeing that all queues are stable. Given queue state $\Theta(t)$ in slot t, we can obtain the optimal transmission decisions by solving the following problem:

$$\begin{aligned}\mathbf{P1:}\ \min_{\mathbf{w}(t),a_i(t),\tau(t),f_{ij}(t)}:\ &\sum_{i=1}^{K}\Big\{\mu_1\Big(\hat{E}_i-E_i(t)\Big)(C_i(t)-H_i(t))\\ &+\mu_2 Q_i(t)(R_{xi}(t)-T_{xi}(t))\Big\}\\ &+\mu_3 Z(t)\tau(t)-V\sum_{i=1}^{K}U(a_i(t))\\ \text{s.t.}\ \ &C4\sim C9. \end{aligned}\tag{22}$$

Since $H_i(t)$ are not convex for $(\tau(t),\mathbf{w}(t))$, **P1** is nonconvex. To address this issue, we decompose **P1** into several subproblems to obtain the optimal arrival rate control, energy beamforming design, speed control of the mobile sink, and routing algorithm, respectively.

2) Rate Control: We may notice that the rate control variable $a_i(t)$ is independent of other variables in the optimization problem **P1**. Therefore, we can derive the optimal rate control scheme by decomposing **P1** into the following subproblem:

$$\begin{aligned}\mathbf{P2:}\ \min_{a_i(t)}:\ &\sum_{i=1}^{K}(\mu_2 Q_i(t)a_i(t)-VU(a_i(t)))\\ \text{s.t.}\ \ &0\le a_i(t)\le A_i(t)\quad \forall i.\end{aligned}\tag{23}$$

Since the network utility function is concave, the objective function is convex for $a_i(t)$. On the other hand, all constraint functions are linear, so **P2** is a standard convex problem that can be efficiently solved by using the KKT conditions.

Lemma 3: If the network utility function is strictly concave, let $\tilde{a}_i(t)$ denote the solution of equation $\mu_2 Q_i(t) - V([\partial U(a_i(t))]/[\partial a_i(t)]) = 0$, then the optimal rate control scheme is $a_i^*(t) = \min((\tilde{a}_i(t))^+, A_i(t))$. If the network utility function is linear, then the optimal rate control scheme is given by

$$a_i^*(t)=\begin{cases}A_i(t), & \text{if } \mu_2 Q_i(t)\le V\\ 0, & \text{otherwise.}\end{cases}\tag{24}$$

Since the first derivative of the utility function is monotonically decreasing with respect to $a_i(t)$, the solution of equation $\mu_2 Q_i(t) - V([\partial U(a_i(t))]/[\partial a_i(t)]) = 0$ decreases as $Q_i(t)$ increases. This indicates that more sensing data will be placed in the data buffer if the length of data queue $Q_i(t)$ is small enough, and *vice versa*.

3) Energy Beamforming Design: As sink s periodically travels along the straight path, only those sensors within the charging area of sink s can receive the RF beams to harvest energy. Therefore, for the beamforming design at each slot, we only take the sensors that can effectively receive RF beams into our design. Let $\mathbf{S}(t)=\mathbf{w}(t)\mathbf{w}(t)^{\mathrm{H}}$ and $\mathbf{G_i}(t)=\mathbf{g_{is}}(t)^{\mathrm{H}}\mathbf{g_{is}}(t)$, so we have $|\mathbf{g_{is}}(t)\mathbf{w}(t)|^2=\mathrm{tr}(\mathbf{G_i}(t)\mathbf{S}(t))$ and $\|\mathbf{w}(t)\|^2=\mathrm{tr}(\mathbf{S}(t))$. To obtain the optimal energy beamforming design, we decompose the optimization problem **P1** into the beamforming design subproblem, which can be equivalently transformed as follows:

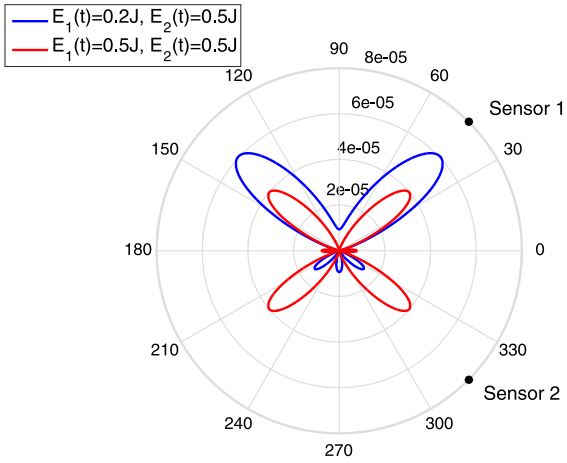

Fig. 3. Antenna radiation patterns of the uniform linear array.

$$\begin{aligned}\mathbf{P3}:\ \min_{\mathbf{w}(t)}:\ &\mu_1\eta\tau(t)\mathrm{tr}(\mathbf{X}(t)\mathbf{S}(t))\\ \text{s.t.}\ \ &0\le\mathrm{tr}(\mathbf{S}(t))\le P_{\max}^{s}\\ &\mathrm{rank}(\mathrm{tr}(\mathbf{S}(t))=1\end{aligned}\tag{25}$$

where $\mathbf{X}(t) = -\sum_{i\in\mathcal{K}(t)}(\hat{E}_i - E_i(t))\mathbf{G_i}(t)$. Since $\hat{E}_i - E_i(t) \ge 0$, $\mathbf{X}(t)$ is a negative semidefinite matrix, which results in $\mathrm{tr}(\mathbf{X}(t)\mathbf{S}(t)) \le 0$. On the other hand, the variables $\tau(t)$ and $\mathbf{w}(t)$ are independent in the feasible set of **P1**, and the value of $\tau(t)$ is always larger than zero. Therefore, $\tau(t)$ will not affect the optimal energy beamforming vector. $\tau(t)$ can be regarded as a constant in the above optimization problem, which will lead to the following lemma.

Lemma 4: The optimal energy beamforming design is given by

$$\mathbf{w}^*(t)=\sqrt{P_{\max}^{s}}\underline{\mathbf{u}}(\mathbf{t})\tag{26}$$

where $\underline{\mathbf{u}}(\mathbf{t})$ is an eigenvector corresponding to the minimum eigenvalue of the matrix $\mathbf{X}(\mathbf{t})$.

Proof: See Appendix C. ■

From the objective function of **P3**, we can observe that $(\hat{E}_i - E_i(t))$ can be regarded as the weighting coefficient of the harvested energy at sensor node i. When $(\hat{E}_i - E_i(t))$ is large enough, $-\mu_1\eta(\hat{E}_i - E_i(t))\tau(t)\mathrm{tr}(\mathbf{G_i}(t)\mathbf{S}(t))$ dominates the value of the objective function. In this case, the sensor i will expect to harvest more energy, and the mobile sink will direct the main energy beams toward sensor i. In other words, if sensor i has a lower energy queue state $E_i(t)$, the main energy beam will be directed to sensor i.

To explore the impact of the energy queuing size on the energy beamforming design, the relationship between $E_i(t)$ and the harvested energy is illustrated in Fig. 3. Here, we assumed that sink s is equipped with four antennas and $\tau(t) = 1$ s. There are two sensors within the charing coverage of sink s. The sensor locations relative to sink s are $d_1 = 5$ m, $\psi_1 = 45°$,

$d_2 = 5$ m, and $\psi_2 = 315°$. The other simulation parameters used are given in Section V. As can be seen from Fig. 3, the energy beam will be focused on sensor 1 when $E_1(t) < E_2(t)$ and even energy can be directed to both sensors when $E_1(t) = E_2(t)$.

4) Speed Control of the Mobile Sink and Routing Design: Since we assume that the distance moved by sink s in each time slot is l, the optimal speed of sink s is determined once we derive the optimal $\tau(t)$. This indicates that we can derive the optimal $\tau(t)$ instead of directly optimizing $v(t)$. When the optimal energy beamforming vector is obtained, the optimal speed of sink s and routing scheme can be derived by solving the following subproblem:

$$\mathbf{P4:}\ \min_{\tau, f_{ij}}:\ -\sum_{i\in\mathcal{K}(t)}\mu_1\Big(\hat{E}_i - E_i(t)\Big)\big|\mathbf{g_{is}}(t)\mathbf{w}^*(t)\big|^2\eta\tau(t) + \mu_3 Z(t)\tau(t) + \sum_{i=1}^{K}\left\{u_1\Big(\hat{E}_i - E_i(t)\Big)C_i(t) + \mu_2 Q_i(t)\times\left(\sum_{j:i\in O(j)} f_{ji}(t) - T_{xi}(t)\right)\right\}$$

$$\text{s.t.}\ \ C4, C7, C8, C9.$$

We can note that the objective and all the constraints function are linear in $\tau(t)$ and $f_{ij}(t)$, and thus **P4** is a standard linear programming problem. Next, we will design a distributed speed control and routing algorithm to obtain the suboptimal solution by using the dual decomposition method, the proximal minimization algorithm, and the subgradient method. Due to the objective function of **P4** is not strictly convex with respect to optimization variables, we cannot obtain the primal solution immediately for the dual problem. First, based on the proximal minimization algorithm [33], we can transform a linear programming problem into a strictly convex quadratic programming problem by adding a quadratic term $c_1\tau^2(t) + c_2\sum_{i=1}^{K}\sum_{j:j\in O(i)\cup\{s\}} f_{ij}^2(t)$ to the objective function. Let $F(f_{ij}(t), \tau(t))$ and $(f_{ij}^*(t), \tau^*(t))$ denote the objective function and optimal solution of **P4**, respectively. The optimal solution of quadratic programming problem is denoted by $(\tilde{f}_{ij}(t), \tilde{\tau}(t))$. Thus, we can obtain

$$\begin{aligned} &F\Big(f_{ij}^*(t), \tau^*(t)\Big) + c_1\tau^{*2}(t) + c_2\sum_{i=1}^{K}\sum_{j:j\in O(i)\cup\{s\}} f_{ij}^{*2}(t) \\ &\quad\geq F\Big(\tilde{f}_{ij}(t), \tilde{\tau}(t)\Big) + c_1\tilde{\tau}^2(t) + c_2\sum_{i=1}^{K}\sum_{j:j\in O(i)\cup\{s\}} \tilde{f}_{ij}^2(t) \qquad (27) \\ &\Rightarrow F\Big(\tilde{f}_{ij}(t), \tilde{\tau}(t)\Big) - F\Big(f_{ij}^*(t), \tau^*(t)\Big) \\ &\quad\leq c_1\left(\left(\frac{l}{\underline{v}}\right)^2 - \left(\frac{l}{\overline{v}}\right)^2\right) + c_2\sum_{i=1}^{K}\sum_{j:j\in O(i)\cup\{s\}}\left(\frac{W_{ij}l}{\underline{v}}\right)^2. \qquad (28) \end{aligned}$$

This implies that $F(\tilde{f}_{ij}(t), \tilde{\tau}(t))$ can arbitrarily approach the optimal value of the original optimization problem **P4** if we choose small enough c_1 and c_2.

Let λ_i^e, λ_i^d, and ξ_{ij} denote the Lagrange multipliers associated with the energy queue constraint of sensor i, data queue constraint at the ith sensor, and the link capacity constraint, respectively. Therefore, the Lagrange dual function is given in (29), shown at the bottom of the page, and the dual problem is expressed as follows:

$$\max_{\boldsymbol{\lambda},\boldsymbol{\xi}}\ : L(\boldsymbol{\lambda}, \boldsymbol{\xi}). \qquad (30)$$

Moreover, we may notice that the dual problem can be further subdivided into $K+1$ independent subproblems when $\boldsymbol{\lambda}$

$$\begin{aligned} L(\boldsymbol{\lambda}, \boldsymbol{\xi}) = \min_{f_{ij}(t),\tau(t)}:\ & c_1\tau^2(t) + c_2\sum_{i=1}^{K}\sum_{j:j\in O(i)\cup\{s\}} f_{ij}^2(t) + \mu_3 Z(t)\tau(t) - \sum_{i\in\mathcal{K}(t)} u_1\Big(\hat{E}_i - E_i(t)\Big)\big|\mathbf{g_{is}}(t)\mathbf{w}^*(t)\big|^2\eta\tau(t) \\ &+ \sum_{i=1}^{K}\left\{\mu_1\Big(\hat{E}_i - E_i(t)\Big)C_i(t) + \mu_2 Q_i(t)\left(\sum_{j:i\in O(j)} f_{ji}(t) - T_{xi}(t)\right)\right\} \\ &+ \sum_{i=1}^{K}\left\{\lambda_i^e(C_i(t) - E_i(t)) + \lambda_i^d(T_{xi}(t) - Q_i(t)) + \sum_{j\in O(i)\cup\{s\}}\xi_{ij}\big(f_{ij}(t) - W_{ij}\tau(t)\big)\right\} \\ =\ & \min_{f_{ij}(t),\tau(t)}:\sum_{i=1}^{K}\left\{\sum_{j:j\in O(i)}\left(\Big(\mu_1\Big(\hat{E}_j - E_j(t)\Big) + \lambda_j^e\Big)E_j^{rx} + \mu_2 Q_j(t)\Big)f_{ij}(t)\right. \\ &\qquad\left. + \sum_{j:j\in O(i)\cup\{s\}}\left(\Big(\mu_1\Big(\hat{E}_i - E_i(t)\Big) + \lambda_i^e\Big)E_{ij}^{tx}(t) - \mu_2 Q_i(t) + \xi_{ij} + \lambda_i^d\Big)f_{ij}(t) + c_2 f_{ij}^2(t)\right\} \\ &+ \left(\mu_3 Z(t) - \sum_{i\in\mathcal{K}(t)} u_1\Big(\hat{E}_i - E_i(t)\Big)\big|\mathbf{g_{is}}(t)\mathbf{w}^*(t)\big|^2\eta - \sum_{i=1}^{K}\sum_{j:j\in O(i)\cup\{s\}}\xi_{ij}W_{ij}\right)\tau(t) \\ &+ c_1\tau^2(t) - \sum_{i=1}^{K}\Big(\lambda_i^e E_i(t) + \lambda_i^d Q_i(t)\Big) \end{aligned} \qquad (29)$$

and $\boldsymbol{\xi}$ are given, which can be expressed as

$$L_i = \min_{f_{ij}(t)}: \sum_{j\in O(i)} \Big(\Big(\mu_1\Big(\hat{E}_j - E_j(t)\Big) + \lambda_j^e\Big)E_j^{rx} + \mu_2 Q_j(t)\Big) f_{ij}(t) + \sum_{j\in O(i)\cup\{s\}} \Big\{\Big(\Big(\mu_1\Big(\hat{E}_i - E_i(t)\Big) + \lambda_i^e\Big)E_{ij}^{tx}(t) - \mu_2 Q_i(t) + \xi_{ij} + \lambda_i^d\Big) f_{ij}(t) + c_2 f_{ij}^2(t)\Big\},\ i = 1, 2, \ldots, K \tag{31}$$

$$L_{K+1} = \min_{\tau(t)}: \left(-\sum_{i\in\mathcal{K}(t)} u_1\Big(\hat{E}_i - E_i(t)\Big)|\mathbf{g_{is}}(t)\mathbf{w}^*(t)|^2\eta - \sum_{i=1}^{K}\sum_{j\in O(i)\cup\{s\}} \xi_{ij}W_{ij} + \mu_3 Z(t)\right)\tau(t) + c_1\tau^2(t). \tag{32}$$

By using the dual decomposition method, the speed control and routing design optimization problem has been decomposed into $K+1$ dual subproblems, the K sensors can solve the corresponding K subproblems to obtain the optimal routing scheme, and sink s can solve the $(K+1)$th subproblem to derive the optimal speed. On this basis, we can present a distributed algorithm by using the subgradient method, which is an iterative process by solving the series of convex quadratic programming until convergence. The detailed procedure is as follows.

Given the initial Lagrange multipliers λ_i^e, λ_i^d, and ξ_{ij}, for the kth iteration, we have the following.

1) The total amount of sensing data $f_{ij}(t)$ transmitted by sensor i is given by

$$f_{ij}^{k+1}(t) = \frac{1}{2c_2}\Big(-\Big(\mu_1\Big(\hat{E}_j - E_j(t)\Big) + \lambda_j^e(k)\Big)E_j^{rx} - \Big(\mu_1\Big(\hat{E}_i - E_i(t)\Big) + \lambda_i^e(k)\Big)E_{ij}^{tx}(t) - \xi_{ij}(k) - \lambda_i^d(k) + \mu_2\big(Q_i(t) - Q_j(t)\big)\Big)^+ \quad \forall j \in O(i) \tag{33}$$

$$f_{is}^{k+1}(t) = \frac{1}{2c_2}\Big(-\Big(\mu_1\Big(\hat{E}_i - E_i(t)\Big) + \lambda_i^e(k)\Big)E_{ij}^{tx}(t) + \mu_2 Q_i(t) - \xi_{ij}(k) - \lambda_i^d(k)\Big)^+. \tag{34}$$

2) The speed of sink s is determined by

$$\tau^{k+1}(t) = \left[\frac{1}{2c_1}\left(\sum_{i\in\mathcal{K}(t)} \mu_1\Big(\hat{E}_i - E_i(t)\Big)\big|\mathbf{g_{is}}(t)\mathbf{w}^*(t)\big|^2\eta + \sum_{i=1}^{K}\sum_{j\in O(i)\cup\{s\}} \xi_{ij}(k)W_{ij} - \mu_3 Z(t)\right)\right]^\dagger \tag{35}$$

where $[\,\cdot\,]^\dagger = \min\{\max\{\cdot, (l/\overline{v})\}, (l/\underline{v})\}$.

3) The Lagrange multipliers are iteratively updated as follows:

$$\lambda_i^e(k+1) = \Big(\lambda_i^e(k) + \delta_i^e(k)\Big(C_i^k(t) - E_i(t)\Big)\Big)^+ \tag{36}$$

$$\lambda_i^d(k+1) = \Big(\lambda_i^d(k) + \delta_i^d(k)\Big(T_{xi}^k(t) - Q_i(t)\Big)\Big)^+ \tag{37}$$

$$\xi_{ij}(k+1) = \Big(\xi_{ij}(k) + \delta_{ij}(k)\Big(f_{ij}^k(t) - W_{ij}\tau^k(t)\Big)\Big)^+ \tag{38}$$

where $\delta_i^e(k)$, $\delta_i^d(k)$, and $\delta_{ij}(k)$ are the step sizes used in the kth iteration, which controls the convergence speed of λ_i^e, λ_i^d, and λ_{ij} toward their optimal values.

We repeat the above iteration until the sequences of $f_{ij}^k(t)$ and $\tau^k(t)$ converge to their optimal solutions.

From (33) and (34), we may find that the total amount of sensing data transmitted by sensor i depends on the energy queue and data queue states of the sensors involved. With the increase in $Q_i(t)$ and $E_i(t)$, the sensing data transmitted by sensor i will be larger. Moreover, $f_{ij}(t)(j \neq s)$ will be larger than zero only when $Q_i(t) > Q_j(t)$, which indicates that only when sensor i has more sensing data than sensor j, sensor j can act as relay to help sensor i forward sensing data. On the other hand, from (35), we may notice that the terms of $\sum_{i\in\mathcal{K}(t)} \mu_1(\hat{E}_i - E_i(t))|\mathbf{g_{is}}(t)\mathbf{w}^*(t)|^2\eta$, $\sum_{i=1}^{K}\sum_{j\in O(i)\cup\{s\}} \xi_{ij}W_{ij}$, and $\mu_3 Z(t)$ jointly determine the speed of sink s. Moreover, $\sum_{i\in\mathcal{K}(t)} \mu_1(\hat{E}_i - E_i(t))|\mathbf{g_{is}}(t)\mathbf{w}^*(t)|^2\eta$ and $\sum_{i=1}^{K}\sum_{j\in O(i)\cup\{s\}} \xi_{ij}W_{ij}$ correspond to the influence by energy harvesting and data transmission, which indicates that a smaller energy queue size or a larger data queue size may result in the lower speed of sink s. Furthermore, we will get a smaller $\tau(t)$ if $Z(t)$ is large enough, which indicates that we should accelerate the speed of sink s to ensure that the average duration of each period will be no larger than T_{tol}.

E. Performance Analysis

In this section, we derive the upper bound on the size of the data queue and the network utility achieved by the proposed ATS.

Theorem 1: When the proposed arrival rate control, energy beamforming design, speed control, as well as distributed routing algorithms are used, for any $V > 0$, there exist $\epsilon > 0$ and $\Psi(\epsilon)$, where $\Psi(\epsilon)$ is smaller than the optimal network utility U^{opt} such that the proposed ATS satisfies the following features.

1) All the data queues $Q_i(t)$, $i = 1, 2, \ldots, K$, and the virtual queue $Z(t)$ are rate stable, so (15) and (16) can be ensured.
2) The network utility and the average data queue size can be bounded by

$$\lim_{M\to\infty}\frac{1}{M}\sum_{t=0}^{M-1}\sum_{k=1}^{K}\mathbb{E}[U(a_k)] \geq U^{\text{opt}} - \frac{\bar{B}}{V} \tag{39}$$

$$\lim_{M\to\infty}\frac{1}{M}\sum_{t=0}^{M-1}\sum_{i=1}^{K}\mathbb{E}[Q_i(t)] \leq \frac{\bar{B} + V\big(U^{\text{opt}} - \Psi(\epsilon)\big)}{\mu_2\epsilon} \tag{40}$$

where

$$\bar{B} = B + c_1\left(\left(\frac{l}{\underline{v}}\right)^2 - \left(\frac{l}{\overline{v}}\right)^2\right) + c_2\sum_{i=1}^{K}\sum_{j:j\in O(i)\cup\{s\}}\left(\frac{W_{ij}l}{\underline{v}}\right)^2. \tag{41}$$

Proof: See Appendix D. ∎

It can be seen from Theorem 1 that the ATS can guarantee the stability of all the data queues and the virtual queue. According to Lemma 1, this means that the sensing data stored

TABLE II
SIMULATION PARAMETER VALUES

Parameter	value	parameter	value
$R_{\max}$	12.5 m	W_{ij}	20 Kbit/s
$\overline{v}$	3 m/s	$\underline{v}$	0.5 m/s
$\hat{E}_i$	1 J	T_{tol}	50 s
E_{elec}	50 nJ/bit	E_{amp}	10 pJ/bit/m^2
l	0.1m	μ_1	10^{10}
μ_2	1	μ_3	10^4

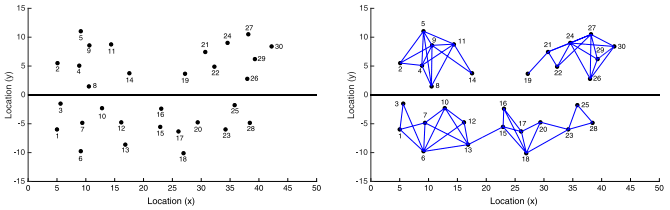

Fig. 4. Topology of RWSN and available routing paths. (a) Network topology. (b) Available routing paths.

in the data buffer will be sent out and the average speed constraint of sink s can be guaranteed. Moreover, the gap between the network utility achieved by the proposed scheme and U^{opt} is inversely proportional to V, and the average data queuing size increases linearly with V. Based on Little's law, the average queuing delay is proportional to the average data queuing size, which shows that the proposed scheme can arbitrarily approach U^{opt} at the expense of a larger queuing delay. Thus, we can realize $[O(1/V), O(V)]$ tradeoff between the network utility and average queuing delay.

V. SIMULATION RESULTS

In this section, we evaluate the transmission performance of the proposed ATS for the RWSN through Monte Carlo simulations. In the simulations, 30 rechargeable sensors are assumed to be randomly deployed in a 25 m×50 m area, and mobile sink s moves along the road ($y_s(t) = 0, x_s(t) \in (0, 50)$) to gather sensing data from these sensors and to charge sensors. Like [3], we set $([G_s G_r \eta P^s_{\max}]/L_p)(\lambda/4\pi)^2 = 4.32 \times 10^{-4}$ and $\beta = 0.2316$, respectively. The average sensing rate of sensor i is set to 500 b/s. The other system simulation parameters and their corresponding values are included in Table II. All the presented simulation results are obtained for $M = 500$ periods.

Fig. 4 illustrates a network topology and the corresponding available paths assumed in the simulation. We assume that the link between sink s and each sensor is always available such that all sensors can send its sensing data directly to mobile sink s. From Fig. 4(b), we may notice that the system requires some sensors near the road to act as relay nodes for other sensors. The initial energy queue state and data queue state for all sensors are set to be zeros. In this article, let the utility function $U(\bar{a}_i) = \log(\bar{a}_i)$ such that the fairness of network can be guaranteed. In order to effectively evaluate the performance of the proposed ATS, we consider sink s with constant speed (CSS) as the benchmark scheme, in which the speed control

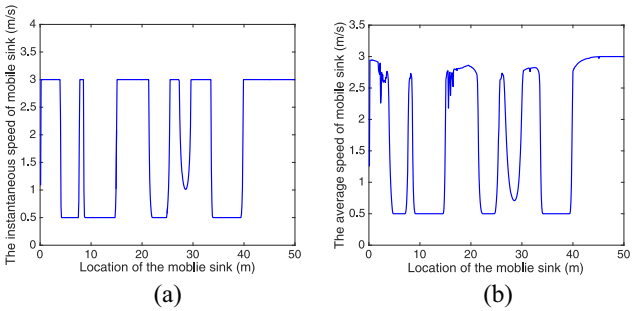

Fig. 5. Speed of sink s at different locations by using the ATS. (a) Instantaneous speed of the mobile sink at the 100th period. (b) Average speed of sink s over 500 periods.

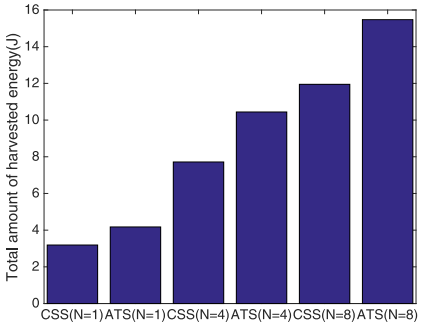

Fig. 6. Total amount of harvested energy by the entire network over 500 periods, $V = 2 \times 10^4$.

of mobile sink in the CSS is independent of the transmission control policy and current data and energy queue states, it may result in a lower transmission efficiency. Based on the proposed ATS algorithm, we only need to set $\overline{v} = \underline{v} = 1$ m/s, the ATS will be reduced to the CSS.

The instantaneous and average moving speed of sink s at different locations are presented in Fig. 5. We can observe that sink s moves along the road only at the maximum speed or the minimum speed in most cases. Besides, combined with the network topology in Fig. 4(a), we can conclude that sink s moves along the road with a lower speed in the dense sensor area and a higher speed in the sparse sensor area. This is because when sink s moves at the minimum speed in the dense sensor area, more energy can be harvested by more sensors such that more sensing data can be gathered by sink s. On the other hand, to ensure the average speed constraint can be satisfied, the mobile sink has to travel at the maximum speed in the sparse sensor area.

The total amount of energy harvested by all sensors and by each sensor over 500 periods for the ATS and CSS with different numbers of antennas are illustrated in Figs. 6 and 7, respectively. We may notice that the harvested energy of the ATS is always larger than that of the CSS. This can be explained by the fact that the proposed ATS can adaptively adjust the speed of mobile sink s. Combined with Figs. 4 and 5, we can observe that the mobile sink travels at a lower speed in the dense sensor area and at a larger speed in the sparse sensor area, which makes sensors harvest more energy. Moreover, the harvested energy will gradually increase with the increase in the number of antennas, as more

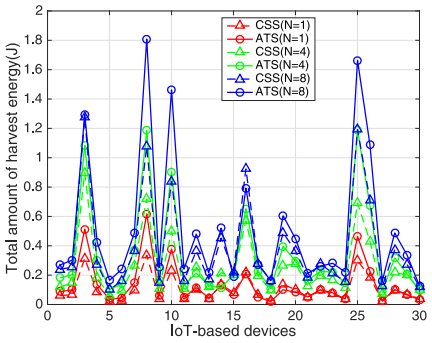

Fig. 7. Total amount of harvested energy by each sensor over 500 periods, $V = 2 \times 10^4$.

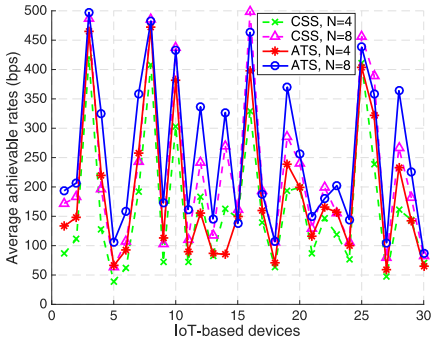

Fig. 8. Average achievable rate for each sensor by different antennas and schemes with $V = 2 \times 10^4$.

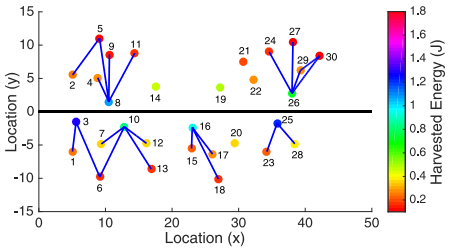

Fig. 9. Routing path for RWSNs by employing CSS with $N = 8$ and $V = 2 \times 10^4$.

energy can be more directed to the desired sensors owing to the energy beamforming design by using multiantenna at mobile sink s. We can observe from Fig. 7 that as expected, sensors close to the road can harvest more energy than others.

Fig. 8 shows the average sensing rate for each sensor employing ATS and CSS with different antennas. We may observe that the ATS has higher sensing rates than the CSS, and the sensing rates will be further improved as the number of antennas increases. Moreover, we can find that the sensors close to the road have higher sensing rates compared to those sensors far away from the road since the "doubly near–far" phenomenon. Therefore, some sensors that are close to the road should act as relays to help other sensors forward sensing data to overcome the "doubly near–far" problem.

Figs. 9 and 10 show the results of the routing path over 500 periods by employing the CSS and ATS, respectively.

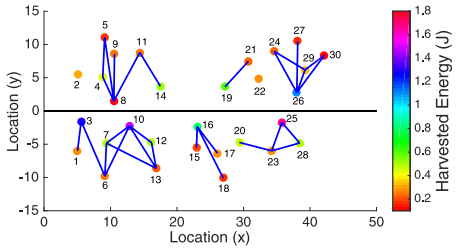

Fig. 10. Routing path for RWSNs by employing ATS with $N = 8$ and $V = 2 \times 10^4$.

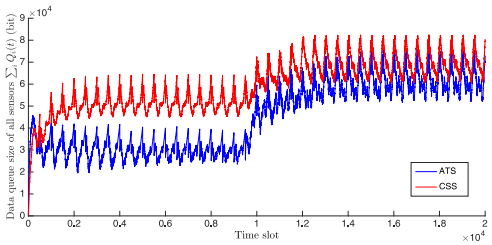

(a)

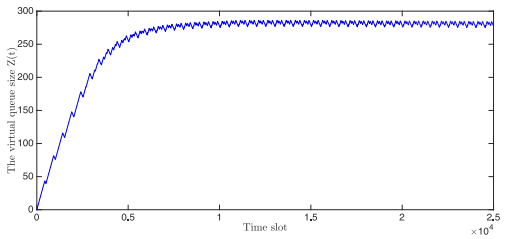

(b)

Fig. 11. Time evolution of the data and virtual queuing size when $N = 4$ and $V = 2 \times 10^4$. (a) Time evolution of the data queuing size. (b) Time evolution of the virtual queuing size.

Compared with Fig. 4(a), we may find that some of the available paths will not be used in 500 periods. This is because, the optimal routing path chosen by each sensor depends on the current energy queue state, data queue state, and its transmission energy. Moreover, we can find that a sensor can be selected as a relay only if its harvested energy is large enough. Taking sensor 6 as an example, there are six available routing paths, but it only chooses two and three links as its routing paths in the CSS and ATS, respectively.

The time evolution of the data and virtual queuing size is shown in Fig. 11. At the first period, the average sensing rate of sensor i is $A_i(t) = 100$ b/s, $i = 1, 2, \ldots, K$. At the 20th period, the average sensing rate of each sensor is changed to $A_i(t) = 500$ b/s. It is observed that both the data and virtual queuing size can quickly achieve new stable states when the sensing rate changes, which implies that the proposed ATS can effectively guarantee the stability of all queues. Moreover, from Fig. 11(a), we can find that there exists an upper bound on the size of the data queue, so when the data buffer size of sensors is large enough, no overflow will occur. Besides, according to Lemma 1, since both the data queue and virtual queue are stable, the average speed constraint of sink s and the flow conservation can be satisfied.

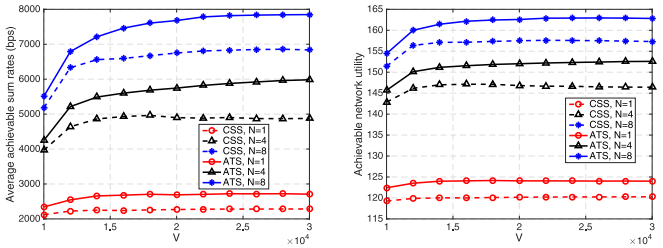

Fig. 12. Achieved performance with different V. (a) Sum rates. (b) Network utility.

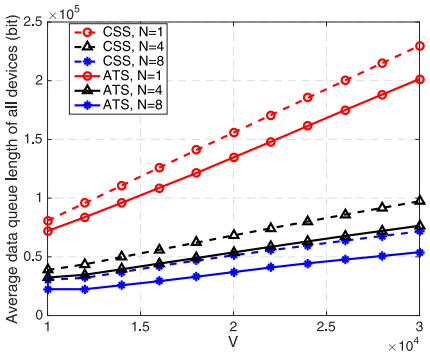

Fig. 13. Average data queuing size with different V.

Fig. 12 presents the effect of different V on the achievable sum rates and network utility. One may observe that the achievable sum rates and network utility increase with the increase in V. Both achievable sum rates and network utility of the ATS are always larger than that of CSS. Moreover, the achieved performance gradually increases with the increase of the number of antennas. This is because ATS can adaptively control the speed of sink s according to the current data and energy queue states, when the sensors around sink s have more sensing data to transmit or have the smaller energy queue size, it will lead to a lower speed. Moreover, the sensors can harvest more energy with an increase in antennas. The relationship between the average data queuing length and V is presented in Fig. 13. We can observe that the average data queuing lengths are proportional to V. All the simulation results are consistent with Theorem 1. This implies that larger achievable network utility and rates can be realized by employing the proposed ATS if a larger queueing delay is tolerable.

VI. Conclusion

In this article, we investigated the wireless energy transfer and data collection problem in RWSNs with a mobile sink. First, the energy beamforming design, rate control, speed control of the mobile sink, and the routing design have been jointly considered in the proposed ATS to maximize the utility of the entire network. Then, we transform the time-average optimization problem into a queue stability one by using the Lyapunov optimization framework and then decompose it into the multiple subproblems by using the optimization decomposition. Moreover, to reduce the computing load of the mobile sink, a distributed speed control and routing algorithm was proposed to obtain the near-optimal solution for data collection. Furthermore, our analysis shows that there is an inherent tradeoff between the network utility and the average queueing size, and the proposed ATS can achieve the near-optimal network utility when a certain queueing delay can be tolerated. Numerical analyses are presented to demonstrate the effectiveness of the proposed ATS. It should be addressed that in this article, we only consider a linear energy harvesting model. In practical systems, the energy conversion efficiency may not be a constant, but a function of the received power, which will lead to a nonlinear energy harvesting model. The nonlinear energy harvesting model and its impact on the adaptive transmission design remain open issues for future investigation.

Appendix A

Based on the data and virtual queue evolution equation (13), (14), we have

$$Q_i(t+1) \geq Q_i(t) + R_{xi}(t) - T_{xi}(t), \quad i = 1, 2, \ldots, K \tag{42}$$

$$Z(t+1) \geq Z(t) + \tau(t) - \frac{T_{\text{tol}}}{N_t}. \tag{43}$$

By summing (42) and (43) over M slots and dividing by M, then taking $\lim_{M\to\infty}$ on both sides, we can obtain

$$\lim_{M\to\infty} \frac{Q_i(M) - Q_i(0)}{M} \geq \lim_{M\to\infty} \frac{1}{M} \sum_{t=0}^{M-1} (R_{xi}(t) - T_{xi}(t)) \tag{44}$$

$$\lim_{M\to\infty} \frac{Z(M) - Z(0)}{M} \geq \lim_{M\to\infty} \frac{1}{M} \sum_{t=0}^{M-1} \tau(t) - \frac{T_{\text{tol}}}{N_T}. \tag{45}$$

Without loss of generality, let the data queue and virtual queue initial states $Q_i(0)$ and $Z(0)$ equal to zero. On the other hand, the data queue and virtual queue are rate stable, i.e., $\lim_{M\to\infty}([Q_i(M)]/M) = \lim_{M\to\infty}[Z(M)/M] = 0$. Therefore, based on (44) and (45), we can yield (15) and (16). This completes the proof of Lemma 1.

Appendix B

From (12)–(14), we have

$$\begin{aligned}\left(\hat{E}_i - E_i(t+1)\right)^2 &\leq \left(\hat{E}_i - E_i(t) - H_i(t) + C_i(t)\right)^2 \\ &\leq \left(\hat{E}_i - E_i(t)\right)^2 + 2\left(\hat{E}_i - E_i(t)\right) \\ &\quad \times (C_i(t) - H_i(t)) + \hat{H}_i^2 + \hat{C}_i^2 \end{aligned} \tag{46}$$

$$Q_i^2(t+1) \leq Q_i^2(t) + 2Q_i(t)(R_{xi}(t) - T_{xi}(t)) + \hat{R}_{xi}^2 + \hat{T}_{xi}^2 \tag{47}$$

$$\begin{aligned}Z^2(t+1) &\leq Z^2(t) + 2Z(t)\left(\tau(t) - \frac{T_{\text{tol}}}{N_T}\right) + \left(\frac{l}{v}\right)^2 \\ &\quad + \left(\frac{T_{\text{tol}}}{N_T}\right)^2. \end{aligned} \tag{48}$$

Combining with (17), (18), and (20), we can obtain Lemma 2.

APPENDIX C

Let $\mathbf{X}(t) = -\sum_{i\in\mathcal{K}(t)}(\hat{E}_i - E_i(t))\mathbf{G_i}(t)$, since $\hat{E}_i - E_i(t) \geq 0$ and $\mathbf{G_i}(t)$ is a symmetric positive semidefinite matrix, then $\mathbf{X}(t)$ is a symmetric negative semidefinite matrix. On the other hand, $\mathbf{S}(t)$ is a symmetric positive semidefinite matrix of rank one, and thus using the eigenvalue decomposition, we have

$$\mathbf{X}(t) = \mathbf{U}(t)\Sigma_{\mathbf{X}}\mathbf{U}(t)^{\mathrm{H}}, \quad \mathbf{S}(t) = \mathbf{V}(t)\Sigma_{\mathbf{S}}\mathbf{V}(t)^{\mathrm{H}} \tag{49}$$

where $\mathbf{U}(t)$ and $\mathbf{V}(t)$ are unitary matrices, and $\Sigma_{\mathbf{X}} = \mathrm{diag}(x_1, x_2, \ldots, x_N)$ and $\Sigma_{\mathbf{S}} = \mathrm{diag}(s_1, 0, \ldots, 0)$ $(s_1 \geq 0)$ are diagonal matrices. Since $\Sigma_{\mathbf{X}}$ is a negative semidefinite diagonal matrix, without loss of generality, we assume that $x_1 \leq x_2 \leq \cdots \leq x_N \leq 0$, and thus we can obtain

$$\begin{aligned}&\mathrm{tr}(\mathbf{X}(t)\mathbf{S}(t)) = \mathrm{tr}\big(\mathbf{U}(t)\Sigma_{\mathbf{X}}\mathbf{U}(t)^{\mathrm{H}}\mathbf{V}(t)\Sigma_{\mathbf{S}}\mathbf{V}(t)^{\mathrm{H}}\big)\\ &\xLeftrightarrow{\mathbf{L}(t)=\mathbf{U}(t)^{\mathrm{H}}\mathbf{V}(t)} \mathrm{tr}\big(\mathbf{L}(t)^{\mathrm{H}}\Sigma_{\mathbf{X}}\mathbf{L}(t)\Sigma_{\mathbf{S}}\big) = s_1\sum_{i=1}^{N} x_i|l_{i1}|^2\end{aligned} \tag{50}$$

where $(l_{11}, l_{21}, \ldots, l_{N1})^{\mathrm{T}}$ is the first column vector of $\mathbf{L}(t)$. since $\mathbf{L}(t)$ is a unitary matrix, we have $\sum_{i=1}^{N} l_{i1} = 1$. Thus, we can derive $\mathrm{tr}(\mathbf{X(t)S(t)}) \geq s_1x_1 \geq P^s_{\max}x_1$. $\mathrm{tr}(\mathbf{X}(t)\mathbf{S}(t))$ can be minimized when $\mathbf{V}(t) = \mathbf{U}(t)$ and $s_1 = P^s_{\max}$, so we can obtain

$$\mathbf{S}(t) = \mathbf{U}(t)\Sigma_{\mathbf{S}}\mathbf{U}(t)^{\mathrm{H}} = P^s_{\max}\underline{\mathbf{u}}(t)\underline{\mathbf{u}}(t)^{\mathrm{H}}. \tag{51}$$

Therefore, the optimal energy beamforming is $\mathbf{w(t)} = \sqrt{P^s_{\max}}\underline{\mathbf{u}}(\mathbf{t})$. This completes the proof of Lemma 4.

APPENDIX D

With the same approach in [34], there exist a stationary randomized rate control, energy beamforming design, speed control, and routing design scheme $(a_i^*(t), \mathbf{w}^*(t), \tau^*(t), f_{ij}^*(t))$, which is independent of $\Theta(t)$ and satisfies the following conditions:

$$\sum_{i=1}^{K}\mathbb{E}\big[U\big(a_i^*(t)\big)|\Theta(t)\big] = \sum_{i=1}^{K}\mathbb{E}\big[U\big(a_i^*(t)\big)\big] = \Psi(\epsilon) \tag{52}$$

$$\mathbb{E}\big[C_i^*(t) - H_i^*(t)|\Theta(t)\big] \leq 0 \quad \forall\ i \tag{53}$$

$$\mathbb{E}\big[R_{xi}^*(t) - T_{xi}^*(t)|\Theta(t)\big] \leq -\epsilon \quad \forall\ i \tag{54}$$

$$\mathbb{E}\left[\tau^*(t) - \frac{T_{tol}}{N_T}|\Theta(t)\right] \leq 0. \tag{55}$$

Moreover, the proposed scheme is expected to minimize the right-hand side of (21), but the proposed distributed speed control and routing algorithm is suboptimal. However, we have derived the maximum gap between the suboptimal solution and the optimal solution in (28). Thus, by substituting (28) and (52)–(55) into (21), we have

$$\begin{aligned}&\Delta(\Theta(t)) - V\sum_{i=1}^{K}\mathbb{E}[U(a_i(t))|\Theta(t)]\\ &\leq \bar{B} - V\Psi(\epsilon) - \epsilon\mu_2\sum_{i=1}^{K}Q_i(t)\end{aligned} \tag{56}$$

where $\bar{B}$ is defined in (41). Taking the expectation for (56), we can obtain

$$\begin{aligned}&\mathbb{E}[L(\Theta(t+1)) - L(\Theta(t))] - V\sum_{i=1}^{K}\mathbb{E}[U(a_i(t)\,]\\ &\leq \bar{B} - V\Psi(\epsilon) - \epsilon\mu_2\sum_{i=1}^{K}\mathbb{E}[Q_i(t)].\end{aligned} \tag{57}$$

Without loss of generality, let $L(\Theta(0)) = 0$. By rearranging the above equation and summing over M slots, we have

$$\frac{\mu_3}{2}\mathbb{E}\Big[Z^2(t)\Big] \leq \bar{B}M + V\left(\sum_{t=0}^{M-1}\sum_{i=1}^{K}\mathbb{E}[U(a_i(t)\,] - \Psi(\epsilon)M\right). \tag{58}$$

Since $\lim_{M\to\infty}(1/M)\sum_{t=0}^{M-1}\sum_{i=1}^{K}\mathbb{E}[U(a_i(t))]$ of the proposed adaptive scheme cannot exceed the optimal U^{opt}, i.e., $\lim_{M\to\infty}(1/M)\sum_{t=0}^{M-1}\sum_{i=1}^{K}\mathbb{E}[U(a_i(t))] \leq U^{\mathrm{opt}}$ and $\mathbb{E}[Z^2(t)] \geq \mathbb{E}[Z(t)]^2$. Therefore, we can obtain

$$\mathbb{E}[Z(t)] \leq \sqrt{\frac{2M\big(\bar{B} + V(U^{\mathrm{opt}} - \Psi(\epsilon))\big)}{\mu_3}}. \tag{59}$$

Taking a limit as $M \to \infty$ and dividing by M for (59), we obtain $\lim_{M\to\infty}[(\mathbb{E}[Z(t)])/M] = 0$. Thus, $Z(t)$ is rate stable and the average speed constraint of sink s will be guaranteed. Moreover, the similar proof process is applied to the data queue $Q_i(t)$, which results in (15) and (16) are satisfied.

By summing (57) over M time slots and dividing it by M, we can obtain

$$\begin{aligned}&\frac{\mathbb{E}[L(\Theta(M))] - \mathbb{E}[L(\Theta(0)\,]}{M} - \frac{V}{M}\sum_{t=0}^{M-1}\sum_{i=1}^{K}\mathbb{E}[U(a_i(t))]\\ &\leq \bar{B} - V\Psi(\epsilon) - \frac{\mu_2\epsilon}{M}\sum_{t=0}^{M-1}\sum_{i=1}^{K}\mathbb{E}[Q_i(t)].\end{aligned} \tag{60}$$

We may notice that $L(\Theta(t)) \geq 0\ \forall t$, we have

$$\frac{1}{M}\sum_{i=1}^{K}\sum_{t=0}^{M-1}\mathbb{E}[U(a_i(t))] \geq \Psi(\epsilon) - \frac{\bar{B}}{V} \tag{61}$$

$$\begin{aligned}\frac{1}{M}\sum_{t=0}^{M-1}\sum_{i=1}^{K}\mathbb{E}[Q_i(t)] \leq \frac{\bar{B} - V\Psi(\epsilon)}{\mu_2\epsilon} + \frac{V}{\mu_2\epsilon M}\\ \times\sum_{t=0}^{M-1}\sum_{i=1}^{K}\mathbb{E}[U(a_i(t))].\end{aligned} \tag{62}$$

Taking a limit as $M \to \infty$ and $\Psi(\epsilon) \to U^{\mathrm{opt}}$ as $\epsilon \to 0$ for (61), we can obtain the network utility as (39). By taking a limit as $M \to \infty$ for (62), we can obtain the upper bound of the average data queue size in (40). This completes the proof of Theorem 1.

REFERENCES

[1] Y. Shi, L. Xie, Y. Hou, and H. Sherali, "On renewable sensor networks with wireless energy transfer," in *Proc. IEEE Conf. Comput. Commun. (INFOCOM)*, 2011, pp. 1350–1358.

[2] L. Xie, Y. Shi, Y. Hou, and H. D. Sherali, "Making sensor networks immortal: An energy-renewal approach with wireless power transfer," *IEEE/ACM Trans. Netw.*, vol. 20, no. 6, pp. 1748–1761, Dec. 2012.

[3] S. He, J. Chen, F. Jiang, D. K. Y. Yau, G. Xing, and Y. Sun, "Energy provisioning in wireless rechargeable sensor networks," *IEEE Trans. Mobile Comput.*, vol. 12, no. 10, pp. 1931–1942, Oct. 2013.

[4] M. Zhao, J. Li, and Y. Yang, "A framework of joint mobile energy replenishment and data gathering in wireless rechargeable sensor networks," *IEEE Trans. Mobile Comput.*, vol. 13, no. 12, pp. 2689–2705, Dec. 2014.

[5] S. Guo, C. Wang, and Y. Yang, "Joint mobile data gathering and energy provisioning in wireless rechargeable sensor networks," *IEEE Trans. Mobile Comput.*, vol. 13, no. 12, pp. 2836–2852, Dec. 2014.

[6] D. Niyato, P. Wang, H. Tan, W. Walid, and D. Kim, "Cooperation in delay-tolerant networks with wireless energy transfer: Performance analysis and optimization," *IEEE Trans. Veh. Technol.*, vol, 64, no. 8, pp. 3740–3754, Aug. 2015.

[7] L. Xie, Y. Shi, Y. T. Hou, W. Lou, H. D. Sherali, and S. F. Midkiff, "Multi-node wireless energy charging in sensor networks," *IEEE/ACM Trans. Netw.*, vol. 23, no. 2, pp. 437–450, Apr. 2015.

[8] L. Fu, L. He, P. Cheng, Y. Gu, J. Pan, and J. Chen, "ESync: Energy synchronized mobile charging in rechargeable wireless sensor networks," *IEEE Trans. Veh. Technol.*, vol. 65, no. 9, pp. 7415–7431, Sep. 2016.

[9] G. Han, X. Yang, L. Liu, and W. Zhang, "A joint energy replenishment and data collection algorithm in wireless rechargeable sensor networks," *IEEE Internet Things J.*, vol. 5, no. 4, pp. 2596–2604, Aug. 2018, doi: 10.1109/JIOT.2017.2784478.

[10] X. Lu, P. Wang, D. Niyato, D. I. Kim, and X. Han, "Wireless networks with RF energy harvesting: A contemporary survey," *IEEE Commun. Surveys Tuts.*, vol. 17, no. 2, pp. 757–789, 2nd Quart., 2015.

[11] A. Mehrabi and K. Kim, "General framework for network throughput maximization in sink-based energy harvesting wireless sensor networks," *IEEE Trans. Mobile Comput.*, vol. 16, no. 7, pp. 1881–1896, Jul. 2017.

[12] A. Mehrabi and K. Kim, "Maximizing data collection throughput on a path in energy harvesting sensor networks using a mobile sink," *IEEE Trans. Mobile Comput.*, vol. 15, no. 3, pp. 690–704, Mar. 2016.

[13] C. Wang, S. Guo, and Y. Yang, "An optimization framework for mobile data collection in energy-harvesting wireless sensor networks," *IEEE Trans. Mobile Comput.*, vol. 15, no. 12, pp. 2969–2986, Dec. 2016.

[14] L. Huang, "Optimal sleep-wake scheduling for energy harvesting smart mobile devices," *IEEE Trans. Mobile Comput.*, vol. 6, no. 5, pp. 1394–1407, May 2017.

[15] Y. Zhang, S. He, and J. Chen, "Near optimal data gathering in rechargeable sensor networks with a mobile sink," *IEEE Trans. Mobile Comput.*, vol. 16, no. 6, pp. 1718–1729, Dec. 2017.

[16] Y. Zhang, S. He, J. Chen, and X. Shen, "Distributed sampling rate control for rechargeable sensor nodes with limited battery capacity," *IEEE Trans. Wireless Commun.*, vol. 12, no. 6, pp. 3096–3106, Jun. 2013.

[17] Y. Zhang, S. He, and J. Chen, "Data gathering optimization by dynamic sensing and routing in rechargeable sensor networks," *IEEE/ACM Trans. Netw.*, vol. 24, no. 3, pp. 1632–1646, Jun. 2016.

[18] X. Lan, Q. Chen, and L. Cai, "Wireless powered buffer-aided communication over *K*-user interference channel," in *Proc. IEEE 88th VTC-Fall*, Chicago, IL, USA, 2018, pp. 1–6.

[19] S. Timotheou, I. Krikidis, G. Zheng, and B. Ottersten, "Beamforming for MISO interference channels with QoS and RF energy transfer," *IEEE Trans. Wireless Commun.*, vol. 13, no. 5, pp. 2646–2658, May 2014.

[20] Q. Sun, G. Zhu, C. Shen, and Z. Zhong, "Joint beamforming design and time allocation for wireless powered communication networks," *IEEE Commun. Lett.*, vol. 18, no. 10, pp. 1783–1786, Oct. 2014.

[21] Q. Shi, L. Liu, W. Xu, and R. Zhang, "Joint transmit beamforming and receive power splitting for MISO SWIPT systems." *IEEE Trans. Wireless Commun.*, vol. 13, no. 6, pp. 3269–3280, Jun. 2014.

[22] M.-M. Zhao, Y. Cai, Q. Shi, B. Champagne, and M.-J. Zhao, "Robust transceiver design for MISO interference channel with energy harvesting," *IEEE Trans. Signal Process.*, vol. 64, no. 17, pp. 4618–4633, Sep. 2016.

[23] K. W. Choi and D. I. Kim, "Stochastic optimal control for wireless powered communication networks," *IEEE Trans. Wireless Commun.*, vol. 15, no. 1, pp. 686–698, Jan. 2016.

[24] Y. Yun, Y. Xia, B. Behdani, and J. Smith, "Distributed algorithm for lifetime maximization in a delay-tolerant wireless sensor network with a mobile sink," *IEEE Trans. Mobile Comput.*, vol. 12, no. 10, pp. 1920–1930, Oct. 2013.

[25] M. Gatzianas and L. Georgiadis, "A distributed algorithm for maximum lifetime routing in sensor networks with mobile sink," *IEEE Trans. Wireless Commun.*, vol. 7, no. 3, pp. 984–994, Mar. 2013.

[26] L. He, Z. Yang, J. Pan, L. Cai, and J. Xu, "Evaluating service disciplines for on-demand mobile data collection in sensor networks," *IEEE Trans. Mobile Comput.*, vol. 13, no. 4, pp. 797–810, Apr. 2014.

[27] L. Lin, N. B. Shroff, and R. Srikant, "Asymptotically optimal energy-aware routing for multihop wireless networks with renewable energy sources," *IEEE/ACM Trans. Netw.*, vol. 15, no. 5, pp. 1021–1034, Oct. 2007.

[28] W. Wang, V. Srinivasan, and K.-C. Chua, "Extending the lifetime of wireless sensor networks through mobile relays," *IEEE/ACM Trans. Netw.*, vol. 16, no. 5, pp. 1108–1120, Oct. 2008.

[29] C. Wang, J. Li, F. Ye, and Y. Yang, "A mobile data gathering framework for wireless rechargeable sensor networks with vehicle movement costs and capacity constraints," *IEEE Trans. Comput.*, vol. 65, no. 8, pp. 2411–2427, Aug. 2016.

[30] T. Li, P. Fan, and K. Letaief, "Energy harvesting sensor networks with a mobile control center: Optimal transmission policy," in *Proc. IEEE Int. Conf. Commun. (ICC)*, 2015, pp. 3528–3533.

[31] Z. Li, Y. Peng, W. Zhang, and D. Qiao, "J-RoC: A joint routing and charging scheme to prolong sensor network lifetime," in *Proc. IEEE 19th Int. Conf. Netw. Protocols.*, 2011, pp. 373–382.

[32] W. R. Heinzelman, A. Chandrakasan, and H. Balakrishnan, "Energy-efficient communication protocol for wireless microsensor networks," in *Proc. IEEE 33rd Annu. Hawaii Int. Conf. Syst. Sci.*, 2000, pp. 1–10.

[33] D. P. Bertsekas and J. N. Tsitsiklis, *Parallel and Distributed Computation: Numerical Methods*. Englewood Cliffs, NJ, USA: Prentice-Hall, 1989.

[34] M. J. Neely, "Stochastic network optimization with application to communication and queueing systems," *Synth. Lectures Commun. Netw.*, vol. 3, no. 1, pp. 1–211, 2010.

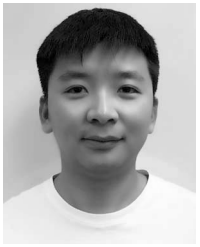

Xiaolong Lan (Member, IEEE) received the B.S. degree in mathematics and applied mathematics from Chengdu University of Technology, Chengdu, China, in 2012, and the Ph.D. degree in information and communication engineering from Southwest Jiaotong University, Shanghai, China, in 2019.

From 2017 to 2019, he was a visiting Ph.D. student with the University of Victoria, Victoria, BC, Canada. He is currently an Associate Researcher with the College of Cybersecurity, Sichuan University, Chengdu. His current research interests include physical layer security, buffer-aided communication, energy-harvesting wireless communication, and mobile-edge computing.

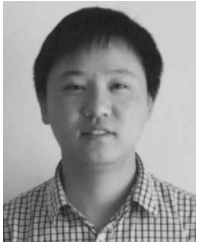

Yongmin Zhang (Member, IEEE) received the Ph.D. degree in control science and engineering from Zhejiang University, Hangzhou, China, in 2015.

He was a visiting student with the California Institute of Technology, Pasadena, CA, USA, and a Postdoctoral Research Fellow with the Department of Electrical and Computer Engineering, University of Victoria, Victoria, BC, Canada. He is currently a Professor with the School of Computer Science and Engineering, Central South University, Changsha, China. His research interests include IoT, smart grid, and mobile computing.

Dr. Zhang won the Best Paper Award of IEEE PIMRC in 2012 and the IEEE Asia–Pacific Outstanding Paper Award in 2018.

Lin Cai (Fellow, IEEE) received the M.A.Sc. and Ph.D. degrees (awarded Outstanding Achievement in Graduate Studies) in electrical and computer engineering from the University of Waterloo, Waterloo, ON, Canada, in 2002 and 2005, respectively.

Since 2005, she has been with the Department of Electrical and Computer Engineering, University of Victoria, Victoria, BC, Canada, where she is currently a Professor. Her research interests span several areas in communications and networking, with a focus on network protocol and architecture design supporting emerging multimedia traffic and the Internet of Things.

Dr. Cai was a recipient of the NSERC Discovery Accelerator Supplement Grants in 2010 and 2015, and the Best Paper Awards of IEEE ICC 2008 and IEEE WCNC 2011. She has co-founded and chaired the IEEE Victoria Section Vehicular Technology and Communications Joint Societies Chapter. She has been elected to serve the IEEE Vehicular Technology Society Board of Governors from 2019 to 2021. She has served as an Area Editor for the IEEE TRANSACTIONS ON VEHICULAR TECHNOLOGY, a member of the Steering Committee for the IEEE TRANSACTIONS ON BIG DATA and the IEEE TRANSACTIONS ON CLOUD COMPUTING, an Associate Editor for the IEEE INTERNET OF THINGS JOURNAL, the IEEE TRANSACTIONS ON WIRELESS COMMUNICATIONS, the IEEE TRANSACTIONS ON VEHICULAR TECHNOLOGY, the IEEE TRANSACTIONS ON COMMUNICATIONS, the *EURASIP Journal on Wireless Communications and Networking*, the *International Journal of Sensor Networks*, and the *Journal of Communications and Networks*, and as the Distinguished Lecturer of the IEEE VTS Society. She has served as a TPC Co-Chair for IEEE VTC2020-Fall and a TPC Symposium Co-Chair for IEEE Globecom'10 and Globecom'13. She is a registered Professional Engineer in British Columbia, Canada. She is an NSERC E.W.R. Steacie Memorial Fellow.

Qingchun Chen (Senior Member, IEEE) received the B.Sc. and M.Sc. degrees (Hons.) from Chongqing University, Chongqing, China, in 1994 and 1997, respectively, and the Ph.D. degree from Southwest Jiaotong University, Chengdu, China, in 2004.

He was with Southwest Jiaotong University from 2004 to 2018. He is currently a Professor with Guangzhou University, Guangzhou, China. He has authored and coauthored over 100 research papers, two book chapters, and 40 patents. His research interests include wireless communication, wireless network, information coding, and signal processing.

Dr. Chen received the IEEE GLOBECOM Best Paper Award in 2016. He has been serving as an Associate Editor for IEEE ACCESS since 2015.